scientific reports

Check for updates

OPEN

Application of HEMA-AAm copolymer to achieve faster optical tissue transparency for 2D/3D fluorescence imaging

Hui Ma[1,2,3,5], Ruixiu Qin[1,3,5], Qiufeng Yao[1,3], Yier Li[1,3], Xingshun Cong[4], Wenhui Wu[2], Qi Zhao[1,3]✉, Hua Ye[1,3]✉ & Kefeng Wu[1,3]✉

Optical transparency methods can facilitate biological tissue optical imaging, which enabled accurate three-dimensional (3D) signal visualization and quantification of complex biological structures. Unfortunately, existing optical clearing approaches present a compromise between maximizing clearing capability, the preservation of fluorescent protein emission and the speed of sample processing. To address this challenge, we synthesis of a 2-hydroxyethyl methacrylate (HEMA)-acrylamide (AAm) copolymer using antipyrine (ATP) and 2,2′-thiodiethanol (TDE) as solvent, which could embed tissue samples rapidly and highly transparent, and compatible with multiple fluorescence labeling. It can enable volumetric imaging of tissue up to the scale of mice organs, shrinkage duration of the clearing and preserve emission from fluorescent proteins and dyes. This copolymer with suitable toughness and plasticity allows the tissue of interest to be sectioned into thin slices, and histological techniques provide high-resolution two-dimensional (2D) images of cells and subcellular structures. Furthermore, HEMA-AAm copolymer -tissue transparent could distinguish cell structures between healthy and diabetic disease in dye-labeled liver tissues, which provides new insights into pathological diagnosis and analysis. Copolymer provides an environment to facilitate high-resolution 3D/2D fluorescence imaging, which enables the study of cellular and tissue morphology in experimental and clinical conditions of interest.

Keywords Copolymer, Optical transparency, Fluorescence imaging

There is a growing demand in the biological field for 3D volume imaging in biological tissues[1]. The study of whole organs or tissues and their cellular components and structures has been historically limited by their natural opacity, which is caused by the optical heterogeneity of the tissue components that scatter light as it traverses through the tissue, and makes 3D tissue imaging highly challenging[2]. The main method of circumventing tissue opacity has been the use of histological tissue sections. While these thin tissue sections can be used to generate precise imaging of subcellular structures, they often lack 3D spatial context and can be subject to tissue deformation and distortions[3]. Recent surges of various tissue clearing techniques open a new era in section-less tissue imaging, enable the precise imaging of cellular and subcellular structures in whole organs and tissues[4]. By combining tissue clearing with optical imaging techniques, 3D images can be generated of entire specimens for visualization and large-scale data analysis[5]. Tissue-clearing techniques and high-resolution volumetric imaging by fluorescence microscopy[6,7] with appropriate fluorescent labeling can provide comprehensive cell information such as cell type, shape, state and distribution of cells of interest throughout an organ[8–12]. In particular, tissue-clearing techniques combined with fluorescence microscopy are a powerful tool to quantify rare cells such as stem cells, metastatic cells or activated neurons in a whole organ for biological research and pathological diagnosis[13].

[1]School of Ocean and Tropical Medicine, Guangdong Medical University, Zhanjiang 524023, People's Republic of China. [2]Department of Marine Bio-Pharmacology, College of Food Science and Technology, Shanghai Ocean University, Shanghai 201306, China. [3]The Marine Biomedical Research Institute of Guangdong Zhanjiang, Zhanjiang 524023, People's Republic of China. [4]Shandong Lunan Coal Chemical Research Institute of Engineering and Technology, Zaozhuang University, Shandong 277160, China. [5]Hui Ma and Ruixiu Qin contributed equally to this work. ✉email: zhaoqi17@mails.ucas.ac.cn; yehua@gdmu.edu.cn; winokhere@sina.com

Tissue clearing techniques reduce the opacity of organs and tissues, to reduce optical scattering and thereby enhance the ability to visualize internal structures in tissue[14,15]. To prepare a transparent organ for volumetric imaging, three major approaches have been reported: hydrophobic, hydrophilic and hydrogel-based tissue-clearing methods. Hydrophobic methods achieve rapid and complete transparency but tend to suppress emission from fluorescent proteins[16–18]. Hydrophilic methods achieve optical transparency with excellent retention of fluorescent proteins emission and capable of preserving detailed structures[19–24], but these approaches are relatively slow (requiring weeks to months to clear cm scale tissue samples)[2,25]. Hydrogel-based approaches involve the transformation of intact tissue into a hydrogel-embedding form[26,27], which can provide high-transparency organs[28], but it is difficult to apply to many samples without dedicated equipment for electrophoresis[29].

Hydrogel-based tissue clearing methods (e.g. CLARITY[30,31], PACT[32,33], SHIELD[34], SWITCH) outstand for the stability and compatibility with bio-molecular staining. The intact biological tissues are substituted with hydrogel polymerization framework, where the proteins, nucleic acids and other macro-biomolecules are immobilized at their native physiological positions while the lipid components remain unbound and are able to be eluted[35,36]. The decrease of lipid barrier increases the penetrability of light and antibodies, allowing the direct stereo imaging of structural and molecular phenotyping of samples. In addition, firm and stable hydrogel environment limits the diffusional contact between the indicator dye and reactive species, thereby improving the shelf life and photochemical stability of the fluorescently labeled specimens, which is particularly important in high-resolution 3D imaging[37]. Also, hydrogel-based tissue clearing methods have irreplaceable advantages in facilitating imaging installation and maintaining tissue morphological structure, but there are still shortcomings, such as long sample processing time and insufficient rigidity of the tissue-gel composite for further sectioning observations[15]. In some studies, it is necessary to acquire high-resolution 2D images of cellular and subcellular at specific locations of interest while maintaining the 3D structure. How to break through these bottlenecks in transparent tissue imaging and achieve comprehensive analysis at both 2D and 3D levels is a new research direction.

Among the tissue-gel co-polymers, the poly-acrylamide gel has long been used in the CLARITY/hydrogel approach to support tissue in the clearing solution for 3D microscopy[38]. However, hydrogels generally possess a soft network, with limited mechanical strength and functions due to the lack of structural complexity. Mechanically strong hydrogels with high toughness have been pursued for decades as candidate materials for soft robotics, tissue replacement[39], or actuators[40]. Enormous efforts have been attempted to fabricate hydrogels with an enhanced mechanical property by using hybrid hydrogels[41,42], Nano-composite hydrogels, or by designing distinctive structures such as an interpenetrating network and dual-cross-linking network. By adjusting the hydrogel's composition, the chemical environment of the tissue-hydrogel complex can be engineered to create a favorable condition for tissue clearing[37,38].

Our research group is dedicated to the development of organizational transparency technologies and applications. In our previous work, we have successfully created a self-assembled DES-based hydrogel for tissues embedding, clearing and imaging[43]. In the present work, we reported the development of copolymer, which is composited of monomers of acrylamide (AAm) and 2-hydroxyethyl methacrylate (HEMA), and 2,2′-thiodiethanol (TDE) and antipyrine (ATP) were used to dissolve monomers. This kind of copolymer overcomes the shortcomings of the existing hydrophilic and hydrogel-based tissue clearing methods, and achieves rapid clearing to high transparency of thick tissues and whole organs while preserving the fluorescent signals and excellent for 3D/2D fluorescence imaging. Additionally, the copolymer enables precise tissue sectioning at interested locations to acquire 2D images of cellular and subcellular structures.

Materials and methods

Antipyrine (ATP), acrylamide (AAm), poly(ethylene glycol) dimethacrylate (PEGDA), 2,2'-azobis[2-(2-imidazolin-2-yl)propane] dihydrochloride (VA-044) were purchased from Shanghai Macklin Biochemical Co., Ltd. Thiodiglycol (TDE) was purchased from Kryptonite Co., Ltd. and 2-hydroxyethyl methacrylate (2-HEMA) was purchased from Aladdin, and all materials were not purified for this experiment. 4% paraformaldehyde (PFA) was provided by Leagene for tissue fixation. The antibodies MAP2, and CD31 and perilipin A were purchased from Signalway Antibody (SAB). The secondary antibodies were purchased from Jackson ImmunoResearch, lectin was purchased from ThermoFisher scientific, and DAPI was purchased from Sigma-Aldrich. Biosharp provided 0.01 M PBS for biological tissue washing.

Wild-type C57BL/6 mice aged 8–12 weeks were purchased from the Guangdong Medical Animal Experiment Center. Enhanced Green Fluorescent Protein (EGFP) mice were purchased from Jiangsu Huachuang Xinnuo Medical Technology Co., Ltd.

Preparation and characterization of HEMA-AAm copolymer

The HEMA-AAm copolymer was synthesized by free-radical polymerization as described in previous reports[44,45]. First, the solution used for dissolving monomers was prepared by mixing the compounds (ATP: TDE in a molar ratio of 1:2). AAm and 2-HEMA as the monomers and PEGDA as the cross-linker, and VA-044 was used as a thermal initiator for thermal polymerization. Monomer solution was prepared by adding 0.9 mL of solution (ATP: TDE = 1:2) with PEGDA (4.9 mg) to a mixture of AAm (0.3 g) and 2-HEMA (0.1 g). Next, 15 µL VA-044 was added and solution was incubated at 37 °C for 12 h to form copolymer gels. The refractive indexes of monomer solution and copolymer were measured by a liquid refractometer and a gem refractometer, respectively.

The texture analysis of the HEMA-AAm copolymer

The structural characteristics of HEMA-AAm copolymer with different monomer proportions were measured using a Texture Analyser (CT3-50 K, America). Cylinder-shaped gel blocks were placed on the TA-BT-KI fixture

base, and the gel testing probe TA39 was selected. Texture Profile Analysis (TPA) mode was employed using the CT5-50 K Texture Analyser for measurement, assessing gel attributes hardness. During the measurement process, the parameters were set as follows: trigger point load of 0.05 N, pre-test speed of 2 mm/s, test speed of 0.1 mm/s, return speed of 4.5 mm/s, data frequency of 10 points per second, and the measurement temperature was maintained at room temperature.

Fourier transform infrared spectra
The freeze-dried HEMA-AAm copolymer was crushed into a powder that was used to prepare KBr pellets. The hydrogel composition and prepolymer solutions were examined by Fourier-transform infrared (FTIR) spectroscopy on a spectrometer (PerkinElmer Spectrum 2000), recorded over the range from 4000 to 400 cm^{-1}.

Scanning electron microscopy (SEM)
The structural morphology of HEMA-AAm copolymer was characterized by scanning electron microscopy. The dried hydrogels for scanning electron microscopy (SEM) were obtained by freeze-drying the hydrogels at – 50 °C (BUCHI L-200 freeze-dryer). Then it was tested by the conductive adhesive bonding method, which is sticking it to the sample stage with conductive adhesive, and the micromorphology of gel was obtained by the Czech TESCAN MIRA LMS.

Rheology
In this study, we characterized the overall viscoelastic behavior of HEMA/AAm copolymers through continuous temperature-sweep rheological experiments. Rheology, the branch of science that focuses on the flow and deformation behavior of materials under external forces, is a key component in material characterization. The viscoelastic properties of materials are commonly examined using rheological experiments. The storage modulus (G') represents the elastic behavior and structural characteristics of a material, reflecting its ability to revert to its original shape after deformation, thus indicating its energy storage capacity. Conversely, the loss modulus (G'') depicts the viscous behavior of a material, showing the energy dissipation during deformation, or its propensity to lose energy. Rheology tests of HEMA-AAm copolymers were conducted using the HAAKE rheometer (Thermofisher/MARSIII). The specific settings were as follows: P35 TiL rotor with a gap set to 1 mm to equilibrate sample for five minutes. Dynamic temperature scans were performed in the temperature range of 25–100 °C at a constant strain of 0.5% and a frequency of 1 Hz, with a heating rate of 5 °C/min.

Animal tissues sample preparation

The mice were fasted for 24 h to reduce the influence of food residue on the experiment. The methods of euthanasia and the agents used for euthanasia and anesthesia are described below: mice were heavily anesthetized with isoflurane and then transcardially perfused with ice cold PBS followed by ice cold 4% PFA in PBS. Mice brains or other tissues were then dissected out and post fixed in 4% PFA overnight at 4 °C. Tissues were stored in PBS with 0.02% sodium azide at 4 °C for further processing.

All animal procedures were conducted in accordance with the National Research Council's Guide for the Care and Use of Laboratory Animals Science, which complied with the ARRIVE guidelines (https://arriveguidelines.org) and U.S. National Institutes of Health (NIH) Guide for the Care and Use of Laboratory Animals. All experiments were approved by the Institutional Animal Care and Use Committee (IACUC) of the Guangdong Laboratory Animals Monitoring Institute (Guangzhou, China, NO. A-IACUC2023104).

Immunostaining
The following primary antibodies were used in this study: CD31 (SAB, dilution 1:50) was selected for labeling of tissue blood vessels; MAP2 was used for immunolabeling of tissue nerves (SAB, dilution 1:50);Perilipin A was used for labeling Lipid droplet-coated proteins. Secondary antibodies including Alexa Fluor® 488-AffiniPure Goat Anti-Mice IgG (H + L)/Alexa Fluor® 488-AffiniPure Goat Anti-Rabbit IgG (H + L)/Alexa Fluor® 647-AffiniPure Goat Anti-Rabbit IgG (H + L) (Jackson ImmunoResearch, dilution 1:100). Took tissues out of the 4% PFA and washed with PBS three times at 37 °C and 50 rpm in a shaker (each time lasted for 1 h). The tissue was immersed in 2% Triton X-100 solution for 1 day at 37 °C, followed by blocking with blocking solution (Beyotime) overnight at 37 °C. The primary antibody was prepared with primary antibody diluent (Beyotime) to the desired concentration and incubated at 37 °C for 48 h in a shaker (50 rpm). The secondary antibody was diluted with secondary antibody diluent (Beyotime) and incubated at 37 °C for 24 h. Then tissue was washed off with PBS three times in the same condition. DAPI (Sigma-Aldrich) was incubated at 37 °C for 12 h to label the nuclei. DyLight 594 Lycopersicon Esculentum (Tomato) lectin (LELDylight 594, Vector Laboratories) was used to label the vasculature through cardiac perfusion. Anaesthetized mice were first perfused with 0.01 M PBS at a rate of 1–2 mL min^{-1}, then perfused with 10–15 mL working solution at a rate of 1–2 mL min^{-1}, finally, the mice were perfused with 4% PFA for fixation. Tissues of interest were harvested and post-fixed in 4% PFA overnight.

Optical tissue clearing method
Briefly, tissues fixed in 4% PFA were washed 3 times with PBS for 1 h each and then immunofluorescence staining of tissues was performed. The stained tissues were immersed in tissue transparency solution at 37 °C for 24 h for tissue clearing. Then the immersed tissues transferred into fresh pre-polymerization solution, after adding VA-044 and polymerization at 37 °C for 24 h to achieve tissue-gel co-transparent. A flow diagram of the tissue clearing process is shown in Fig. S1.

Frozen sectioning of tissue-gel co-transparent

After 3D imaging, the tissue-gel co-transparent was removed from the imaging solution, embedded in OCT compound, and placed on the freezing stage of a cryostat (LEICA CM 1950) until it solidified and could not fall off the sample holder. The temperature of the cryostat was adjusted to -20 °C to -25 °C, and the frozen tissue-gel block was secured on the microtome. Subsequently, it was sectioned into 30–50 μm thick slices, which were then mounted onto glass slides for further microscopic observation.

Fluorescence imaging

2-HEMA/AAm copolymer hydrogels were employed to fix the mice tissue to form tissue-gel co-transparent substance for subsequent imaging. 2D and 3D fluorescence images of transparent tissues were obtained using confocal microscope (IXplore spinSR, Olympus, Japan) and Light Sheet Microscope (Nuohai LS18) to visualize immunostaining and EGFP fluorescence signals. The confocal microscope was used for 2D fluorescence imaging of tissues, while the LSFM was used for acquiring 3D tissue images, allowing the observation of the integrity and fine structure of fluorescence signals within the tissue.

Measurement and quantification of fluorescence intensity

For the analysis of EGFP fluorescence intensity retention, EGFP transgenic mice intestine images were acquired at the same position by super-resolution spinning-disk confocal microscopy on 0, 1, 3, 5 ,7 and 14 days after clearing with hydrogels method. The mean intensity of small intestine cell was measured manually using Fiji. All fluorescence signals were normalized based on day 0 (Day 0 refers to the time of tissue-gel co-transparent complex formation).

Data processing

The data in the figure and legend of the manuscript are presented as mean ± standard deviation (x ± s). Statistical analysis was conducted using t-tests or one-way analysis of variance (ANOVA) as appropriate. Statistical analyses were performed using Image J, GraphPad Prism and origin, 3D reconstruction was performed using AIVIA.

Results and discussion

Copolymer preparation and characterization

In developing hydrogel-based tissue clearing method, we considered how to optimize transparency, ease of operation and fluorescence retention. After screening a number of small molecule substances, ATP and TDE and were found to be most effective in clearing and refractive index (RI) matching. ATP with a high refractive index (RI = 1.585), has been reported as an effective substance for refractive index matching[35]. ATP with aromatic amide group contributed to RI homogenization and high clearing performance because of their efficient solvation of protein backbone amides. Also, ATP avoided tissue shrinkage, even with a dense solution, because this chemical causes tissue swelling[13]. The refractive index of TDE is 1.519–1.523, its refractive index can be adjusted over a wide range, enabling perfect matching between the medium and the sample[46]. Moreover, TDE reduces tissue opacity in a concentration-dependent manner. TDE is suitable for various applications and imaging techniques, which is compatible with immunostaining and can preserves fluorescence without cause deformations at sub-cellular level[47–49]. Interestingly, there was no discernible correlation between the RI values of the medium and tissue transparency, indicating that clearing performance is not solely dependent on the RI value of the medium. In our experiments, we synergistically incorporated ATP and TED, meticulously adjusting their concentrations to achieve enhanced tissue optical transparency. This optimization took into account both the refractive index and the efficiency of the clearing process. Based on ATP and TED solvents, the tough and high refractive index copolymer were prepared by radical copolymerization of AAm with HEMA monomers in the presence of cross-linker (PEGDA), as shown in Fig. 1, and the specific diagram is shown in the Fig. S2. The effect of different total monomer percentage on the properties of copolymer hydrogels was determined (Table S1). When the polymer monomer percentage was less than 10% (w/v), it could not be fully polymerized into a gel. When the polymer monomer percentage was 20–30% (w/v), the gel was too soft to facilitate subsequent sectioning operations. When the monomer content was too high, greater than 40%, the solution content was relatively low and the refractive index decreases, which is unfavorable for tissue transparency. We also found that

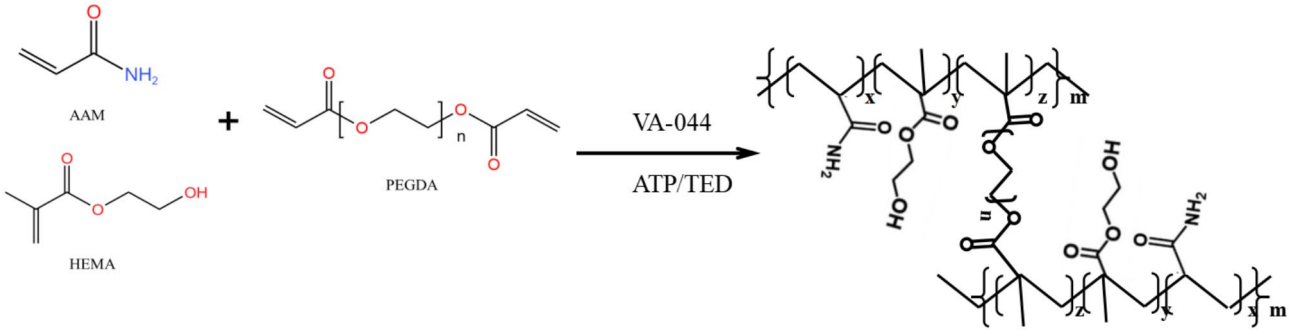

Fig. 1. Synthesis and preparation of HEMA-AAm copolymer.

as the percentage of HEMA increased, the toughness of the hydrogel increased. Finally, we determined that the total monomer percentage remained at 40% (w/v) and HEMA remained at 10% (w/v) for further study.

The successful polymerization was confirmed by FTIR spectra of the copolymer and prepolymer solutions in Fig. 2a. In the prepolymer solutions FTIR spectra, a peak that occured at 1670 cm^{-1} is attributed to the C=C stretching, the peak at 1422 cm^{-1} and 650 cm^{-1} for the C – H bending of alkenes groups. The solution copolymerization to copolymer is confirmed by characteristic absorption of peak at 2921 cm^{-1} for C–H stretching, 1483 cm^{-1} for the C –H bending and 1174 cm^{-1} for the C–C stretching of alkanes groups in the hydrogel FTIR spectra.

To evaluate the mechanical performance of the copolymer, the rheological measurements were presented in Fig. 2b, the HEMA-AAm copolymer showed constant G' and G" values and the relationship of G' > G" in the tested temperature region. This suggested that the HEMA-AAm copolymer had high elastic properties.

Figure 2c shows the SEM images of the freeze-dried fresh, tightly and uniformly packed structures can be found obviously, with a fibre-like structure embedded into a 3D polymeric network. Previous reports indicate that HEMA with a methacrylic group is more reactive than AAm with an acrylic group during radical copolymerization due to the production of tertiary radicals, the HEMA-AAm copolymer hydrogels preferentially consume HEMA and form a relatively dense and rigid network structure at the beginning of the reaction[41,50]. Subsequently, the close association and assembly of AAm in the hydrogels caused dense packing of the polymer. This result was consistent with the fluorescence labeling in Fig. 2d. The synthesis of high strength and toughness hydrogels lays the foundation for subsequent preparation of tissue gel co-transparent composite slices.

HEMA-AAm copolymer are very chemically stable (long shelf life) with strong mechanical strength (provided mainly by HEMA monomer content) to protect the cleared 3D specimen in transport and imaging. Figure S3 shows that after 14 days of exposure to room temperature air, there was no significant change in the transparency of the hydrogels, and no substance precipitated. Furthermore, the DiI dye is stable and uniformly distributed in hydrogels (Fig. S4) with a shelf life. These all allow transfer of 3D specimens among laboratories for offsite imaging and/or tissue preservation and archiving, alleviating facility and time constraints in 3D tissue analysis.

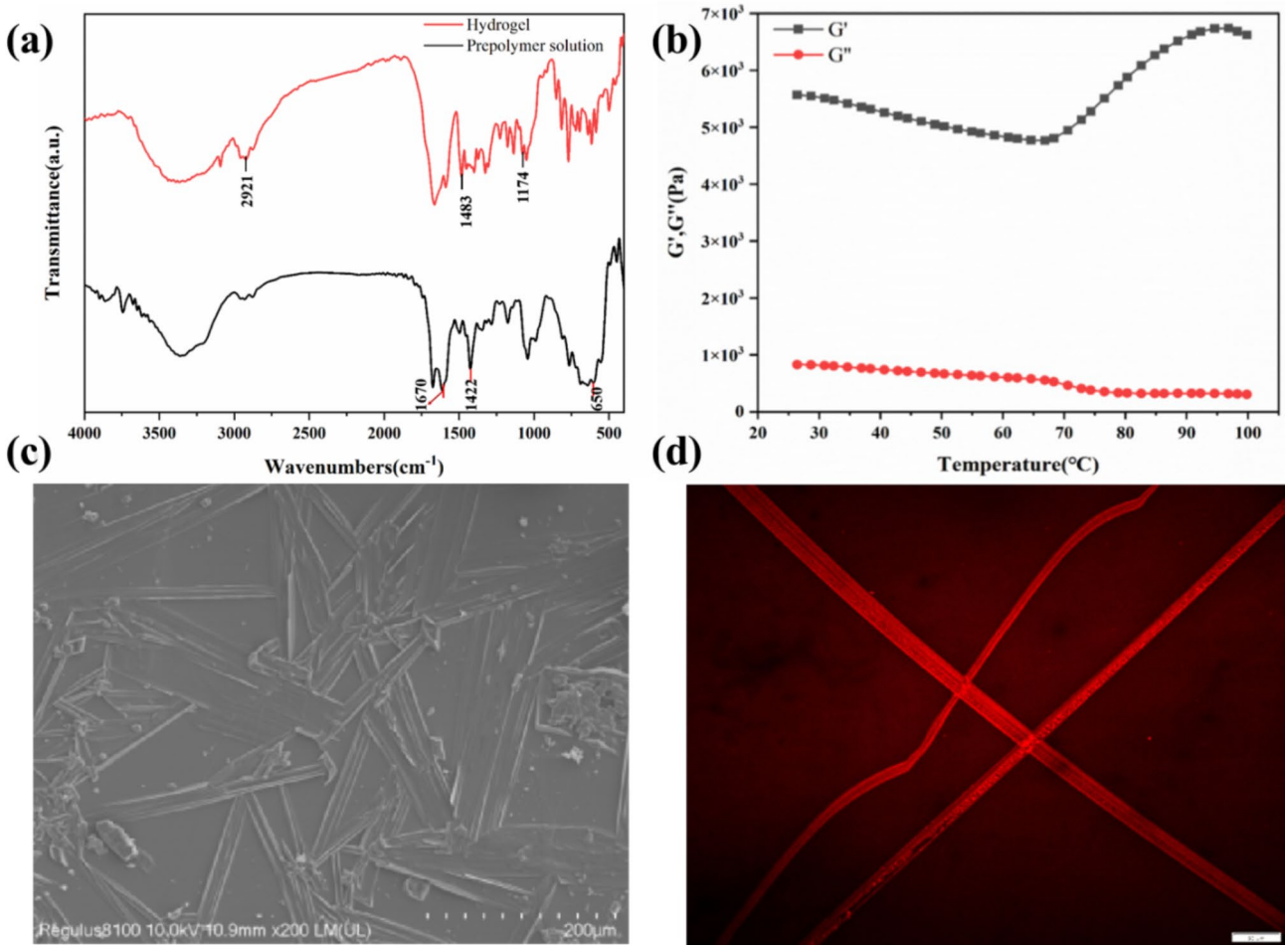

Fig. 2. (a) FT-IR spectra of prepolymer solution and copolymer; (b) HEMA-AAm copolymer rheological behavior analysis. (c) The SEM image and (d) CLSM images of HEMA-AAm copolymer magnified.

Optical clearing of biological tissue

To illustrate the practical performance of hydrogels for organ/tissue imaging, Fig. 3a shows the clearing achieved for various organs/tissue (e.g. heart, liver, spleen, lung, kidney, brain, esophagus and small intestine; $n = 3$), and the intact macro-structures of the embedded intestine tissues in the HEMA-AAm copolymer was shown in Fig. S5. All tissues became high transparent using the HEMA-AAm copolymer, and the final transparency was different among the tissue-gel co-transparent complex. Furthermore, we measured the light transmittance of the tissue before and after clearing, which can visually demonstrate the clearing effect of this method (Fig. S6). HEMA-AAm copolymer has excellent clearing effects on thin-walled tubular organs, such as the small intestine and esophagus. It also demonstrates promising clearing capabilities for thicker parenchymal organs like the liver, spleen, and lung. However, for organs with thick outer walls and complex structures, the tissue clearing effect is not significant, but better transparency can be achieved by simple immersion based on delipidation. In general, the brain is a lipid-rich tissue, and the lungs, esophagus and intestine have luminal structures, heme-rich tissues such as the heart, kidney, and spleen are thicker and denser, these structures probably affect the clearing tendency in optical tissue clearing. Furthermore, different organs have different compositions of lipids, proteins, and extracellular matrix, which mainly affect the performance of tissue clearing.

Shortening the processing time of optical tissue-clearing methods holds practical importance. A high degree of transparency was obtained within a few days (~2–4 days depending on the organ) with minimal volume variation (~110%) (Fig. S7). To clear ~cm scale tissue samples, such as a mice brain hemisphere, requires ~4 days, which is faster than PACT (~7 days) and TESOS (~weeks) shown in Fig. 3b. The PACT tissue clearing method requires A4P0 penetration, polymerization, delipidation and refractive index matching to achieve tissue transparency, which takes at least twice as long as the copolymerized gel method[33]. The TESOS tissue clearing method involves steps such as decolorization, gradient delipidation, dehydration, and refractive index matching, and ultimately the tissue reaches a transparent state in about a few weeks[35]. In contrast, our new copolymer gels method simplifies the clearing procedure and reduces the time required for tissue transparency, achieving tissue transparency in about 4 days.

Copolymer compatibility with fluorescent dyes

The capability of fluorescence retain in tissues clearing is a crucial aspect of tissue clearing technology, we first examined HEMA-AAm copolymer compatible with general methods such as immunofluorescence and EGFP without cell morphology disorganization. The compatibility of with Confocal Laser Scanning Microscopy (CLSM) imaging is shown in Fig. 4. At the tissue level, the copolymer hydrogels cleared mice small intestine with nuclear and neurovascular labeling is prominently seen under the high resolution confocal microscope. The increase in transmittance enables in-depth fluorescence imaging of neurons (MAP2, green), endothelial cell (CD31, green), blood vessels (lectin, red), and nuclei (DAPI stain, blue) and lipid droplet-encapsulated proteins (perilipin A, magenta). In particular, we specified the detailed nervous and endothelial structures.

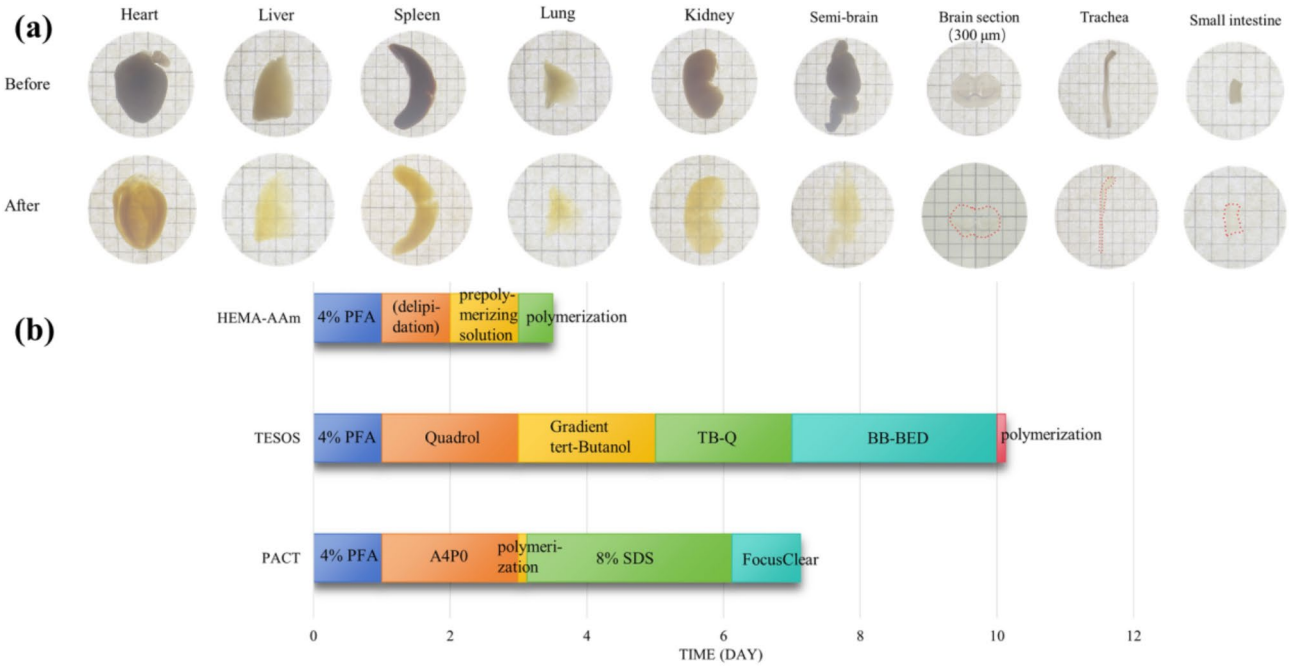

Fig. 3. (a) HEMA-AAm copolymer optical clearing for various tissues (i) Raw samples; (ii) After clearing. (b) Schedules and clearing time comparison of different gel-based clearing methods. (Note: TB-Q dehydration medium was composed of 70% (v/v) tert-Butanol and 30% (w/v) Quadrol; BB-BED clearing medium was composed of 47%(v/v) benzyl benzoate (BB), 48% (v/v) of bisphenol-Aethoxylate diacrylate Mn 468 (BED468) and 5% (v/v) Quadrol.)

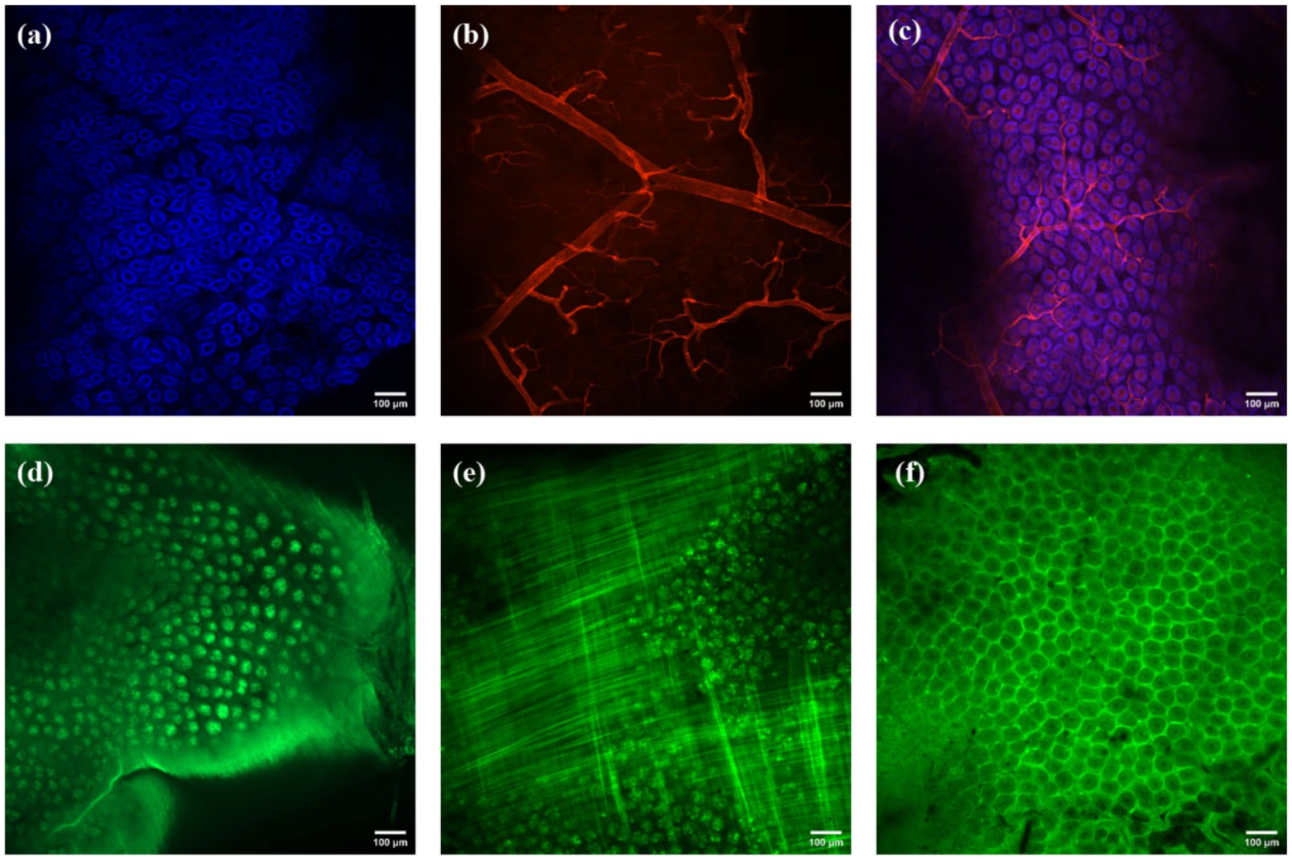

Fig. 4. Fluorescence signals labeled by various chemical fluorescent tracers after HEMA-AAm copolymer optical clearing, including (a) DAPI; (b) Lectin; (c) DAPI and Lectin merged; (d) CD31 antibody, (e) endogenous EGFP signals, and (f) MAP2 antibody.

To examine preservation of EGFP signals after copolymer hydrogels clearing, the mice small intestine samples from EGFP transgenic mice were processed with this methods and images were taken daily at the same position over time as shown in Fig. 5a-f. Normalized fluorescence intensity curves of images taken daily after clearing method, normalized to the signals on day 0 (Fig. 5g). The results showed that more than 75% of the fluorescence signal was preserved even after 3 days, which was significantly preservation. These results all confirmed hydrogels had a good compatibility with both immunofluorescence and autofluorescence.

3D vascular system imaging and reconstruction

We demonstrate the utility of the copolymer clearing method by combining it with laser scanning confocal fluorescence microscopy and light sheet microscopy for 3D imaging of mm-scale tissue blocks and intact whole-organ samples. Figure 6a shows the 3D image of a 2-mm-thick small intestine tissues labled with CD31 and DAPI using CLSM imaging, and Fig. 6b shows higher resolution CLSM images of the same sample. Figure 6c shows the 3D image intestine tissues labled with Lectin and DAPI using light sheet microscopy. We found that after clearing with hydrogels, DAPI-labled nuclei structures and lectin-labeled vascular in the whole mice intestine were well resolved with LSFM imaging. Realizing an efficient and fine reconstruction was one of the important applications, to further examine it, the mice intestine slices were immunofluorescent labeled and treated with copolymer hydrogels. Figure 6d shows the 3D reconstruction of detailed vascular tree networks of the intestine. Furthermore, to demonstrate whole organ imaging, the intact lung lobes of EGFP mice were applied to provide whole-organ clearing and volumetric imaging. Notably, 3D bright fluorescent images of lung sample in Fig. 7 shows the shape and vein of the trachea.

2D imaging obtained though tissue-gel co-transparent slices

After demonstrating the possibility of performing complete volumetric imaging and reconstructions of large volumes at high resolution, we aimed at getting an expanded view of morphological details of mice tissues. In this study, we utilized HEMA-AAm copolymer hydrogel to construct a strong 3D polymer work to prepare tough hydrogel for section. In conjunction with conventional frozen sectioning methods, we performed direct sectioned tissue-gel co-transparent complexes with a thickness of up to 50–100 μm, followed by 2D imaging using super-resolution confocal microscopy. Figure 8 presents 2D fluorescence images of small intestine tissue sections after immunolabeled and gel-embedded, which reveals a clear CD31-labeled vascular endothelium and DAPI-labled nuclei structures. The fluorescence retention of the thin sections is high, the quenching is not

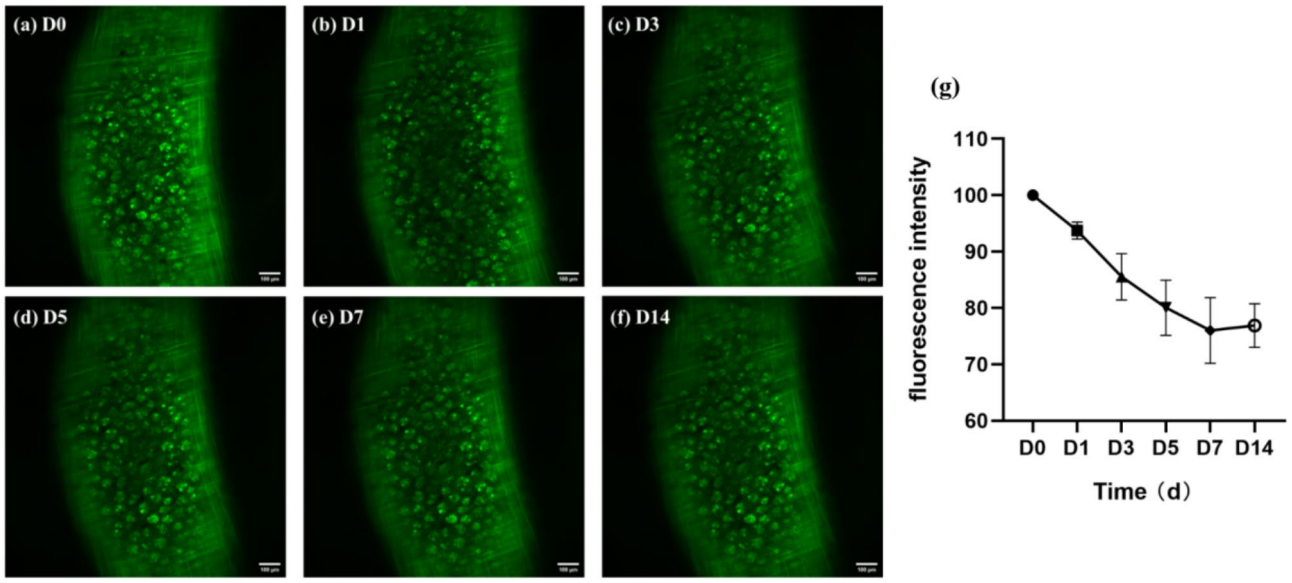

Fig. 5. Fluorescence images of EGFP small intestine at different time points. The fluorescence imaging on (a) day 0; (b) day 1; (c) day 3; (d) day 5; (e) day 7; and (f) day 14 after optical clearing by CLSM scanning; (g) quantification of fluorescence preservation of EGFP after HEMA-AAm copolymer optical clearing.

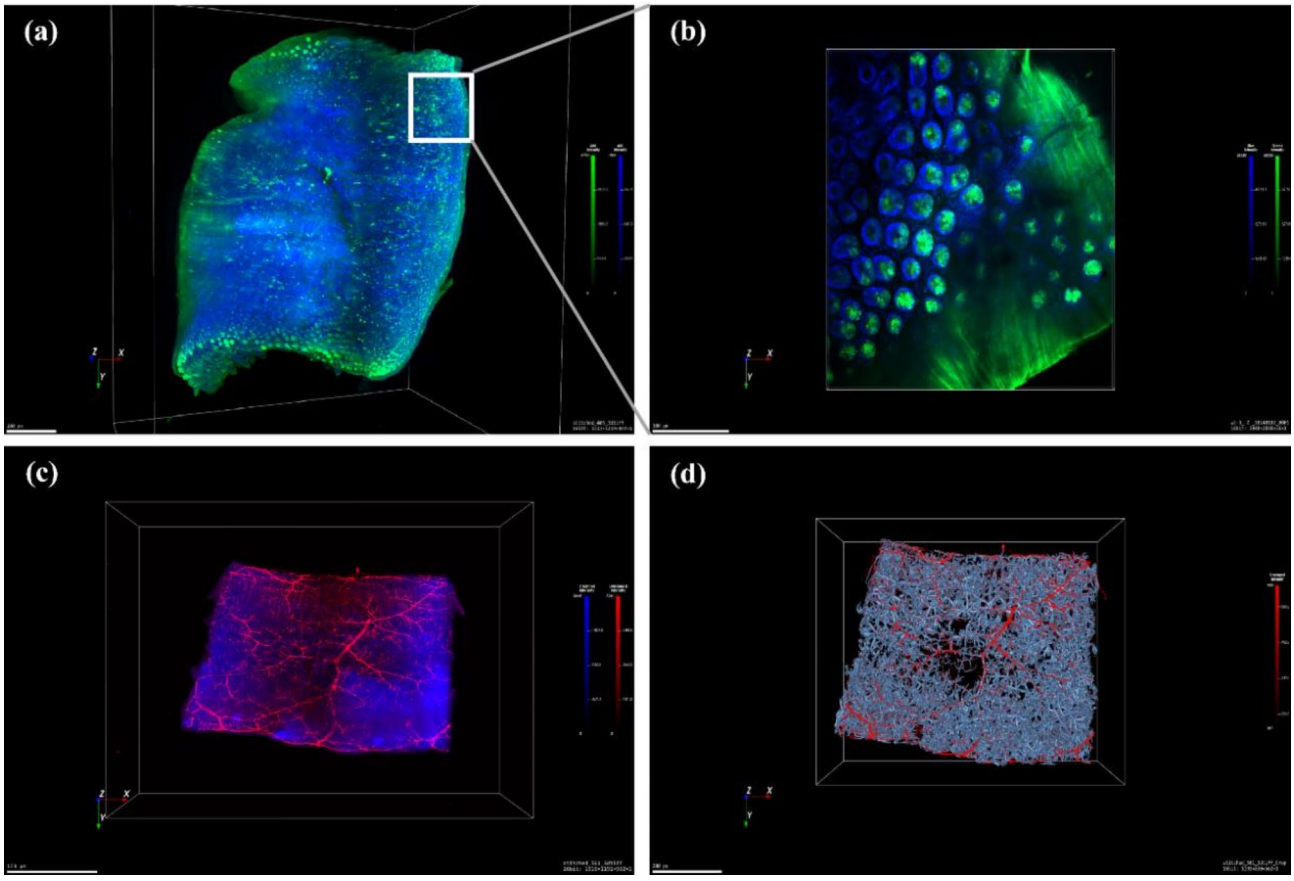

Fig. 6. 3D visualization of small intestine labeled with CD31 and DAPI, (a) 6.3X, LSFM and (b) 10X, CLSM; (c) labeled with Lectin and DAPI, 6.3X, LSFM; (d) 3D reconstruction of small intestinal vascular network achieved by AIVIA.

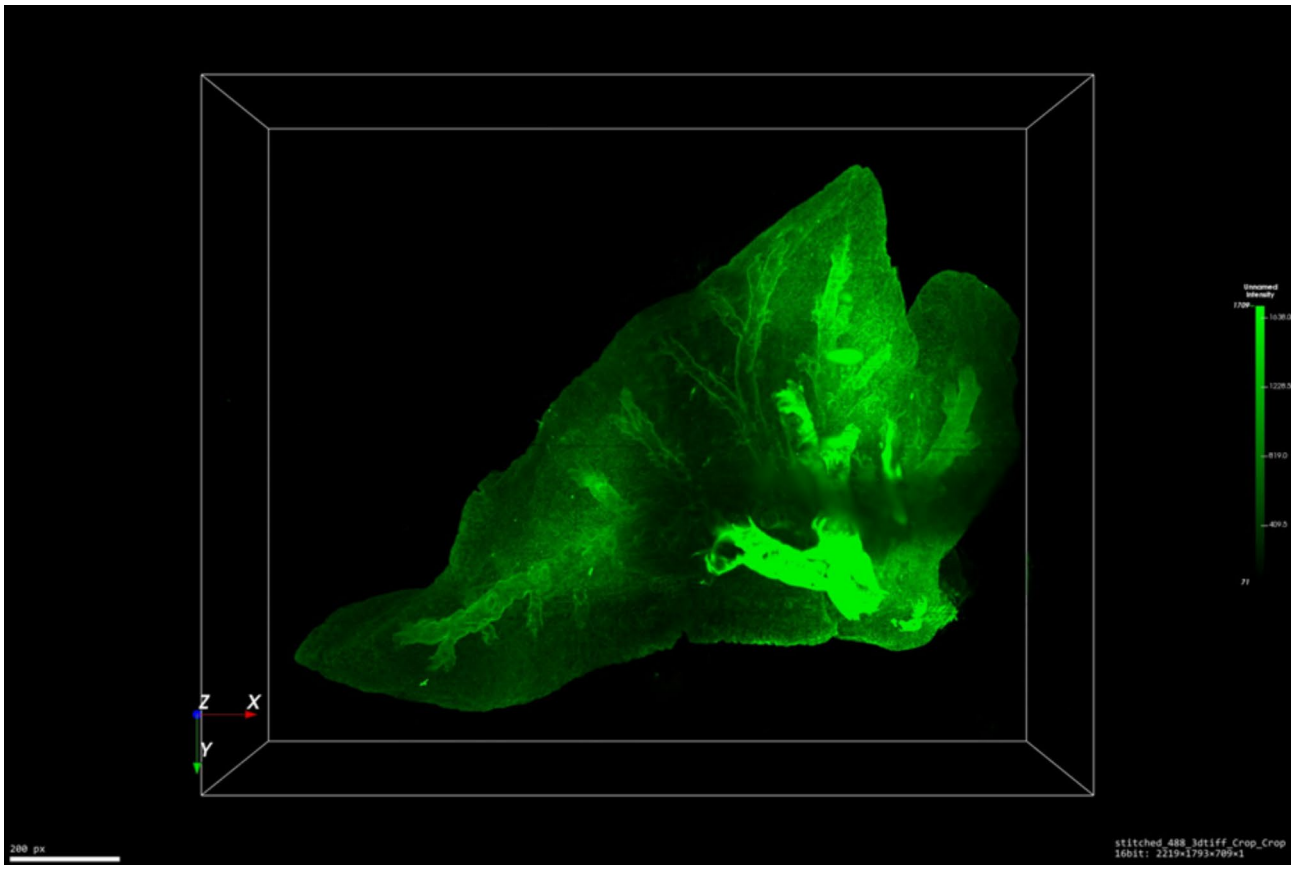

Fig. 7. 3D visualization of EGFP fluorescent murine lung lobes.

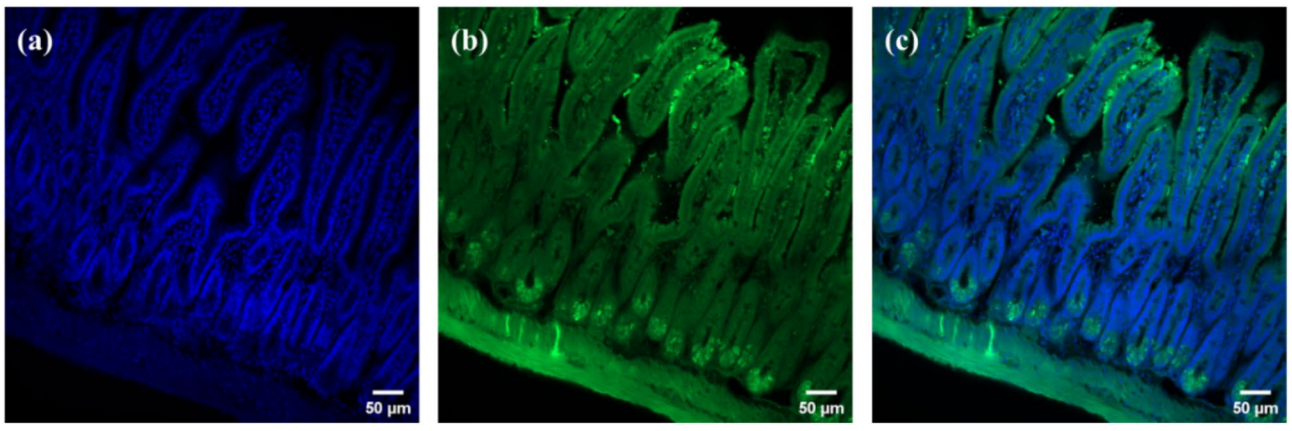

Fig. 8. 3D to 2D retrospection for immunofluorescent imaging. The image of small intestine section labeled with (a) DAPI; (b) CD31; and (c) the merge of CD31 and DAPI signals.

obvious, and the images at the two-dimensional level show more detailed information about the expression of CD31. This characteristic of hydrogels makes them highly advantageous in applied to the field of biomedical imaging, providing new perspectives for tissue physiological or pathological study. Immunolabeling is a powerful tool for biological research and medical diagnosis. In order to map molecular composition and morphology of biomedical specimens, it is usually necessary to mechanically section tissue.

2D detailed cellular structures in health and diabetic disease

We further showed that the morphological analysis of 2D slices to resolve the dye-labeled liver tissue and cellular structures in health and diabetic disease. After immunolabeled with Lectin, DAPI, MAP2 and perilipin A, 2D liver slices of tissue-gel co-transparent sample maintain tissue integrity for CLSM imaging as shown in

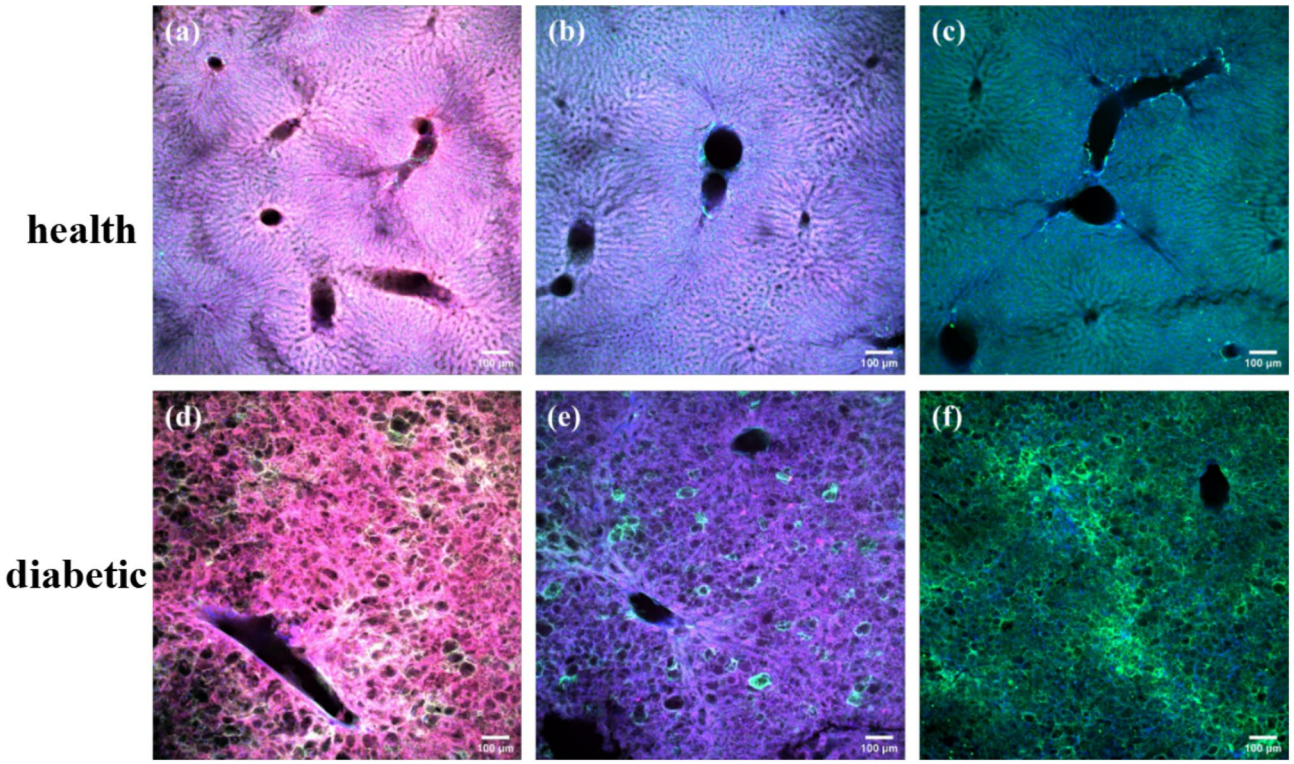

Fig. 9. Fluorescence imaging of liver slice tissues of normal mice and diabetic mice. (a) and (d) are DAPI/MAP2/Lectin/perilipin A merged images; (b) and (e) are DAPI/MAP2/perilipin A merged images; (c) and (f) are DAPI/MAP2 merged image.

Fig. 9. DAPI enables labeling of cell nuclei, and Lectin immunolabeled the intrahepatic blood vasculature was visualized, and intrahepatic nerves were with MAP2 as well as adipocytes with perilipin A. Liver tissue of healthy mice was normal and clear, whereas diffuse lesions without significant parts, changes in the peripheral vessel loop and lipid accumulation were observed in diabetic liver tissue. It offers the interesting possibility of studying proteins, lipids and RNA simultaneously in the diabetic liver micro-environment. This further confirms the potential of the innovative clearing method based on HEMA-AAm copolymer hydrogel for pathological model analysis, providing novel insights for pathological diagnosis and analysis.

Conclusion

High-resolution 3D fluorescence imaging prefers stable chemical and optical conditions to resolve the dye-labeled tissue and cellular structures in health and disease, the intrinsic volatility and molecular diffusion of liquids limit the current approach and design for 3D histology. Here, using the HEMA-AAm copolymer, we created a transparent environment for 3D tissue imaging in a solvent-free condition. The tissue embedding was made possible by thermal-polymerization at 37 °C in ATP/TDE solution, minimizing concerns of tissue damage in a harsh condition of polymer synthesis. HEMA-AAm copolymer is a fast and effective hydrogel-based optical clearing method scalable for various tissues, which can make samples highly transparent in a fairly short time. For instance, the copolymer requires only ~ 4 days clearing a whole ~ cm scale tissue samples, saving almost 75% and 150% of the time needed for PACT and TESOS. Importantly, using the experimental specimens, we established the organ-to-nucleus and panoramic-to-super-resolution imaging, respectively, confirming the intact macro- and micro-structures of the embedded tissues in the HEMA-AAm copolymer. We demonstrated the effectiveness of this method in different applications: in fixed samples by imaging a whole mice lung; in combination with reconstructing the vascular system of the mouse small intestine with light sheet microscopy and in translational research by imaging immunostained mice intestine tissue. By adjusting the HEMA and AAm monomer content appropriately, it achieved refractive index matching with various tissues. The copolymer had suitable toughness and hardness enabling sectioning and preparation of tissue slice for 2D histopathological analysis after 3D imaging. Particularly, using the livers of diabetic mice, we demonstrated the matched lesion microenvironment in the stereomicroscopic and fluorescence, highlighting the 3D/2D imaging with the HEMA-AAm copolymer in experimental related setting. Due to the indicator dyes are stable in the copolymer, the improved shelf life allows transfer of 3D specimens among laboratories for off-site imaging (e.g., at microscope center) and/or tissue preservation and archiving, alleviating the constraints of facility and time in tissue analysis. Overall, this solid environment offers a friendly and versatile platform that integrates with standard fluorescent dye labeling, 2D histology, and 3D super-resolution imaging for investigation of the cellular structures and neurovascular networks in health and disease.

Data availability

The authors declare that the data supporting the findings of this study are available within the paper and its Supplementary Information files.

Received: 25 October 2024; Accepted: 13 March 2025
Published online: 03 April 2025

References

1. Booth, M. J., Neil, M. A. A., Juškaitis, R. & Wilson, T. Adaptive aberration correction in a confocal microscope. *Proc. Natl .Acad. Sci.* **99**, 5788 (2002).
2. Kim, K. et al. Optimized single-step optical clearing solution for 3D volume imaging of biological structures. *Commun. Biol.* **5**, 431 (2022).
3. Ariel, P. A beginner's guide to tissue clearing. *Int. J. Biochem. Cell Biol.* **84**, 35 (2017).
4. Tainaka, K., Kuno, A., Kubota, S. I., Murakami, T. & Ueda, H. R. Chemical principles in tissue clearing and staining protocols for Whole-Body cell profiling. *Annu. Rev. Cell Dev. Biol.* **32**, 713 (2016).
5. Jalufka, F. L. et al. Hydrophobic and hydrogel-based methods for passive tissue clearing. *Fluoresc. Microsc.* **2**, 197 (2022).
6. Voie, A. H., Burns, D. H. & Spelman, F. A. Orthogonal-plane fluorescence optical sectioning: three-dimensional imaging of macroscopic biological specimens. *J. Microsc.* **170**, 22 (1993).
7. Dodt, H. U. et al. Ultramicroscopy: three-dimensional visualization of neuronal networks in the whole mouse brain. *Nat. Methods* **4**, 331 (2007).
8. Kim, Y. et al. Mapping social behavior-induced brain activation at cellular resolution in the mouse. *Cell. Rep.* **10**, 292 (2015).
9. Tomer, R. et al. SPED light sheet microscopy: fast mapping of biological system structure and function. *Cell* **163**, 1796 (2015).
10. Kubota, S. I. et al. Whole-Body profiling of cancer metastasis with Single-Cell resolution. *Cell. Rep.* **20**, 236 (2017).
11. Nojima, S. et al. CUBIC pathology: three-dimensional imaging for pathological diagnosis. *Sci. Rep.* **7**, 9269 (2017).
12. Glaser, A. K. et al. Light-sheet microscopy for slide-free non-destructive pathology of large clinical specimens. *Nat. Biomedical Eng.* **1**, 187 (2017).
13. Murakami, T. C. et al. A three-dimensional single-cell-resolution whole-brain atlas using CUBIC-X expansion microscopy and tissue clearing. *Nat. Neurosci.* **21**, 625 (2018).
14. Chen, L. et al. UbasM: an effective balanced optical clearing method for intact biomedical imaging. *Sci. Rep.* **7**, 12218 (2017).
15. Mai, H. & Lu, D. Tissue clearing and its applications in human tissues: a review. *View* **5**, 368 (2024).
16. Pan, C. et al. Shrinkage-mediated imaging of entire organs and organisms using uDISCO. *Nat. Methods* **13**, 859 (2016).
17. Ertürk, A. et al. Three-dimensional imaging of solvent-cleared organs using 3DISCO. *Nat. Protoc.* **7**, 198 (2012).
18. Dekkers, J. F. et al. High-resolution 3D imaging of fixed and cleared organoids. *Nat. Protoc.* **14**, 1756 (2019).
19. Hama, H. et al. Scale: a chemical approach for fluorescence imaging and reconstruction of transparent mouse brain. *Nat. Neurosci.* **14**, 1481 (2011).
20. Hama, H. et al. ScaleS: an optical clearing palette for biological imaging. *Nat. Neurosci.* **18**, 1518 (2015).
21. Susaki, E. A. et al. Whole-brain imaging with single-cell resolution using chemical cocktails and computational analysis. *Cell* **157**, 726 (2014).
22. Susaki, E. A. et al. Advanced CUBIC protocols for whole-brain and whole-body clearing and imaging. *Nat. Protoc.* **10**, 1709 (2015).
23. Ke, M. T., Fujimoto, S. & Imai, T. SeeDB: a simple and morphology-preserving optical clearing agent for neuronal circuit reconstruction. *Nat. Neurosci.* **16**, 1154 (2013).
24. Kuwajima, T. et al. ClearT: a detergent- and solvent-free clearing method for neuronal and non-neuronal tissue. *Dev. (Cambrid. Engl.)* **140**, 1364 (2013).
25. Hou, B. et al. Scalable and DiI-compatible optical clearance of the mammalian brain. *Front. Neuroanat.* **9**, 19 (2015).
26. Chung, K. et al. Structural and molecular interrogation of intact biological systems. *Nature* **497**, 332 (2013).
27. Murray, E. et al. Simple, scalable proteomic imaging for high-dimensional profiling of intact systems. *Cell* **163**, 1500 (2015).
28. Tomer, R., Ye, L., Hsueh, B. & Deisseroth, K. Advanced CLARITY for rapid and high-resolution imaging of intact tissues. *Nat. Protoc.* **9**, 1682 (2014).
29. Costantini, I. et al. A versatile clearing agent for multi-modal brain imaging. *Sci. Rep.* **5**, 9808 (2015).
30. Jensen, K. H. R. & Berg, R. W. Advances and perspectives in tissue clearing using CLARITY. *J. Chem. Neuroanat.* **86**, 19 (2017).
31. Chung, K. & Deisseroth, K. CLARITY for mapping the nervous system. *Nat. Methods* **10**, 508 (2013).
32. Treweek, J. B. et al. Whole-body tissue stabilization and selective extractions via tissue-hydrogel hybrids for high-resolution intact circuit mapping and phenotyping. *Nat. Protoc.* **10**, 1860 (2015).
33. Yang, B. et al. Single-cell phenotyping within transparent intact tissue through whole-body clearing. *Cell* **158**, 945 (2014).
34. Park, Y. G. et al. Protection of tissue physicochemical properties using polyfunctional crosslinkers. *Nat. Biotechnol.* **6**, 289 (2018).
35. Hsiao, F. T. et al. Transparent tissue in solid state for solvent-free and antifade 3D imaging. *Nat. Commun.* **14**, 3395 (2023).
36. Borchers, A. & Pieler, T. Programming pluripotent precursor cells derived from xenopus embryos to generate specific tissues and organs. *Genes* **1**, 413 (2010).
37. Kojima, C. et al. Application of zwitterionic polymer hydrogels to optical tissue clearing for 3D fluorescence imaging. *Macromol. Biosci.* **21**, 170 (2021).
38. Ono, Y., Nakase, I., Matsumoto, A. & Kojima, C. Rapid optical tissue clearing using poly(acrylamide-co-styrenesulfonate) hydrogels for three-dimensional imaging. *J. Biomed. Mater. Res. B* **107**, 2297 (2019).
39. Ishihara, K., Oda, H. & Konno, T. Spontaneously and reversibly forming phospholipid polymer hydrogels as a matrix for cell engineering. *Biomaterials* **230**, 119628 (2020).
40. Ishihara, K. et al. Biomimetic-engineered silicone hydrogel contact lens materials. *ACS Appl. Bio Mater.* **6**, 3600 (2023).
41. Dohi, S., Suzuki, Y. & Matsumoto, A. One-shot radical polymerization of vinyl monomers with different reactivity accompanying spontaneous delay of polymerization for the synthesis of double-network hydrogels. *Polym. Int.* **69**, 954 (2020).
42. Li, J. et al. Hofmeister effect mediated strong PHEMA-Gelatin hydrogel actuator. *ACS Appl. Mater. Interfaces.* **6**, 269 (2022).
43. Ruixiu Qin, P. H. et al. Supramolecular self-assembling hydrogel based on imidazole/d-sorbitol deep eutectic solvent for tissue clearance. *J. Mol. Liquids* **3**, 409 (2024).
44. Koda, T. et al. One-shot preparation of polyacrylamide/poly(sodium styrenesulfonate) double-network hydrogels for rapid optical tissue clearing. *ACS Omega* **4**, 21083 (2019).
45. Qin, H. & Panzer, M. J. Chemically cross-linked poly(2-hydroxyethyl methacrylate)-supported deep eutectic solvent gel electrolytes for eco-friendly supercapacitors. *ChemElectroChem* **4**, 2556. (2017).
46. Musielak, T. J., Slane, D., Liebig, C. & Bayer, M. A versatile optical clearing protocol for deep tissue imaging of fluorescent proteins in Arabidopsis Thaliana. *PloS One* **11**, 161107 (2016).
47. Staudt, T., Lang, M. C., Medda, R., Engelhardt, J. & Hell, S. W. 2,2'-thiodiethanol: a new water soluble mounting medium for high resolution optical microscopy. *Microsc. Res. Tech.* **70**, 1 (2007).
48. Appleton, P. L., Quyn, A. J., Swift, S. & Näthke, I. Preparation of wholemount mouse intestine for high-resolution three-dimensional imaging using two-photon microscopy. *J. Microsc.* **234**, 196 (2009).

49. Gonzalez-Bellido, P. T. & Wardill, T. J. Labeling and confocal imaging of neurons in thick invertebrate tissue samples. *Cold Spring Harbor Protocols* **2012**, 969. (2012).
50. Dei, N., Ishihara, K., Matsumoto, A. & Kojima, C. Preparation and characterization of acrylic and methacrylic Phospholipid-Mimetic polymer hydrogels and their applications in optical tissue clearing. *Polymers* **16**, 241 (2024).

Acknowledgements

This work was supported by the Fund of Southern Marine Science and Engineering Guangdong Laboratory (Zhanjiang) (ZJW-2019-007), the Special Funds for Economic Development of Marine Economy of Guangdong Province, China (GDME-2018C011), the Special Science and Technology Innovation Project of Guangdong Province, China (2019A01005, 2019A03023). Natural Science Foundation of Shandong Province (ZR2023QB205) and (ZR2022MB027), and Youth Research Projects of Guangdong Medical University (GDMUD2024005).

Author contributions

CRediT authorship contribution statement Hui Ma: Data curation, Writing–original draft， Methodology. Ruixiu Qin: Investigation, Methodology, Data curation. Qiufeng Yao: Methodology, Formal analysis. Yier Li: Formal analysis, Software. Xingshun Cong: Investigation, Software. Hua Ye: Supervision, Resources. Qi Zhao: Project administration, Writing–review & editing. Wenhui Wu: Validation, Visualization, Conceptualization. Kefeng Wu: Funding acquisition, Resources, Supervision, Writing–review & editing.

Competing interests

The authors declare no competing interests.

Additional information

Supplementary Information The online version contains supplementary material available at https://doi.org/10.1038/s41598-025-94479-z.

Correspondence and requests for materials should be addressed to Q.Z., H.Y. or K.W.